A comparative study on two stress intensity factor-based criteria for prediction of mode-I crack propagation in concrete

Wei Dong[1], Zhimin Wu[2,*], Xiangming Zhou[3], Cuijin Wang[4]

[1]Associate Professor, State Key Laboratory of Coastal and Offshore Engineering, Dalian University of Technology, Dalian 116024, P. R. China. E-mail: dongwei@dlut.edu.cn

[2]Professor, State Key Laboratory of Coastal and Offshore Engineering, Dalian University of Technology, Dalian 116024, P. R. China.

(*Corresponding author). E-mail: wuzhimin@dlut.edu.cn

[3]Senior lecturer, Department of Mechanical, Aerospace and Civil Engineering, Brunel University, London, UB8 3PH, UK & Haitian Visiting Professor, State Key Laboratory of Coastal and Offshore Engineering, Dalian University of Technology, Dalian 116024, P. R. China. E-mail: xiangming.zhou@brunel.ac.uk

[4]Postgratuate student, State Key Laboratory of Coastal and Offshore Engineering, Dalian University of Technology, Dalian 116024, P. R. China. E-mail: WTQ818@163.com

ABSTRACT

In the analysis of mode-I crack propagation of normal strength concrete at a crack tip, the initial fracture toughness and nil-stress intensity factor (nil-SIF) are two distinguished and widely adopted types of crack propagation criteria. However, there is little information reported on the difference resulting from the two criteria when they are employed to analyze concrete with different strength grades. Aiming at this objective, three-point bending tests are carried out on notched concrete beams of five strength grades, i.e. C20, C40, C60, C80 and C100, and an arrange of initial crack length/depth ratios as 0.2, 0.3 and 0.4, to investigate initial fracture toughness, fracture energy and load-crack mouth opening displacement (P-CMOD) relationship. The two aforementioned types of concrete crack propagation criteria are introduced to determine crack propagation and predict the *P-CMOD* curves of a series of notched concrete beams under a three-point bending test. It has been found that the *P-CMOD* curves calculated using the initial fracture toughness criterion show a better agreement with experimental results than the ones calculated using the nil SIF criterion. With the increase of concrete strength, the difference between the peak loads from experiment and those from analyses based on the nil-SIF criterion becomes increasingly larger than the scenarios based on the initial fracture toughness criterion. Therefore, it can be reasonably concluded that for the two types of concrete crack propagation criteria, the initial fracture toughness is more appropriate for describing the fracture behavior of concrete, especially for high strength concrete.

Keywords: Concrete; mode-I fracture; crack propagation process; crack propagation criterion; initial fracture toughness

1. Introduction

The cracking process in quasi-brittle materials such as concrete and other cement-based composites is usually characterized by the formation of micro-cracks that eventually merge and form a propagating macro-crack. The region where the micro-cracks distribute and the damages accumulate as fracture proceeds is called the fracture process zone (FPZ), which reflects the nonlinear characteristic of concrete as a quasi-brittle material. Due to the existence of FPZ ahead of the crack tip, the whole fracture process in concrete can be divided into three stages, i.e., crack initiation, stable and unstable crack propagation. Effective modelling of the crack initiation and propagation process is significant for assurance of a concrete structures safety and durability.

Since the introduction of the fictitious crack model[1], it has been widely used for simulating the fracture process of concrete and other cement-based materials. In addition, in order to predict crack propagation, an appropriate criterion is a prerequisite for determining crack propagation in concrete. Together with the fictitious crack model, there are three other types of propagation criteria commonly used in the fracture analyses of concrete, i.e., stress-based, energy-based, and stress intensity factor (SIF)-based. Considering that the size of the plastic zone in the fictitious crack is very small for concrete, the maximum tensile stress criterion was proposed as the crack propagation criterion to determine crack propagation in concrete [2-4]. Meanwhile, based on the principle of energy conservation, Xie derived the energy-based cohesive crack propagation criterion for concrete [5] which states that a crack propagates when the strain energy release rate exceeds the energy dissipation rate in FPZ. The criterion has been successfully utilized to simulate crack propagation in concrete [6-8].

On the other hand, the SIF-based crack propagation criteria are also widely adopted in fracture analyses of concrete. In general, based on the linear superposition theory, crack propagation can be determined by assessing the difference of SIFs caused by the driving force and that caused by cohesive forces acting in the FPZ of concrete. It represents the competition between the crack driving force attempting to open the crack and the cohesive force attempting to close it. However, it should be noted that different points of view exist in the research community on the assessment of the difference in SIFs caused by cohesive forces and an applied load in crack propagation criteria. One of them is the nil SIF criterion [9]. Considering that the stress singularity at the fictitious crack tip is removed, a crack can propagate when the SIF caused by the driving force exceeds the one by the cohesive force, i.e. $K_I \geq 0$. This criterion has been used to simulate crack propagation in reinforced concrete [10], mode-I and mixed-mode fracture [11, 12] and multiple cohesive crack propagation [13] in concrete. However, Foot et al. [14] proposed that mortar can be sufficiently characterized by its critical toughness K_m so that all SIFs should refer to the continuous matrix at the crack tip of concrete. Therefore, a critical toughness criterion based on SIFs was proposed, in which a crack can propagate when the difference between the SIF's caused by the driving force and the one by cohesive force exceeds the critical toughness of mortar, i.e. $K_I \geq K_m$. This criterion has been used to simulate crack propagation of mode-I fracture [15, 16] and construct the resistance curve of cement-based composites through numerical analyses [17]. Later, considering concrete as a homogeneous material at a macro-level rather than various distinguished phases at a micro-level, an initial fracture toughness K_{ini} criterion based on

SIFs is proposed [18, 19]. In this criterion, the crack can propagate when the difference of SIF, i.e. K_I, caused by the driving force and the one by the cohesive force exceeds the initial fracture toughness of concrete, i.e. $K_I \geq K_{ini}$. This criterion has been employed to calculate the resistance curve [18], variation of PFZ during the fracture process[20] as well as simulation of crack propagation of mode-I [19, 21] and I-II mixed fracture[18] in concrete.

Although different expressions have been adopted in the three different SIF-based concrete crack propagation criteria discussed above, reasonable agreements have been achieved between model predictions and experimental results for normal strength concrete using all three different crack propagation criteria. It may be because that the values of K_m and K_{ini} in the critical and initial fracture toughness criteria are not large enough to dramatically affect the fracture behavior of normal strength concrete. With the increase of strength, concrete brittleness will increase significantly, resulting in shortening of the PFZ length and enhancement of K_m and K_{ini}. In modelling mode-I crack propagation of normal strength concrete, both crack propagation criteria are appropriate to predict load-crack mouth opening displacement (P-CMOD) curves of notched concrete beams. However, no research has been reported when the SIF-based criteria are employed to determine crack propagation of concrete with different strength grades, especially for high strength concrete. In line with this, the principle objective of the paper is to present a comparative study on the simulation of the whole concrete crack propagation process using the two SIF-based criteria, namely the initial fracture toughness and the nil SIF at the tip of crack. By comparing the P-CMOD curves obtained from experiment and numerical analyses of notched concrete beams with various strength grades, the applicability of the two propagation criteria on mode-I fracture for low, normal and high strength concrete are evaluated. It is expected that the experimental and theoretical investigations presented here will lead to a better understanding of which crack propagation criteria is able to more effectively determine crack propagation for concrete with different strength grades so that a reasonable criterion can be selected in analyzing failure behaviors of structures in practical engineering design.

2. Initial fracture toughness and nil-SIF criteria

According to the fictitious crack model [1], the cohesive stress σ acting on the crack surface of FPZ is very often formulated with respect to crack opening displacement *w.* Based on the linear superposition theory, the SIF at the crack tip in a three-point bending notched beam (Span×Width×Height=$S\times B\times D$) with an initial crack length a_0 can be evaluated using Eq. (1) [22]. The superposition algorithm for calculating K_P and K_σ adopted in this research is schematically illustrated in Fig. 1, in which a crack propagation length Δa is assumed in each analysis step with cohesive stress σ(x) acting on it.

$$K_I=K_P+K_\sigma \tag{1}$$

where, K_P is the SIF caused by the applied load *P, and* K_σ (negative) is the SIF caused by cohesive stress along FPZ.

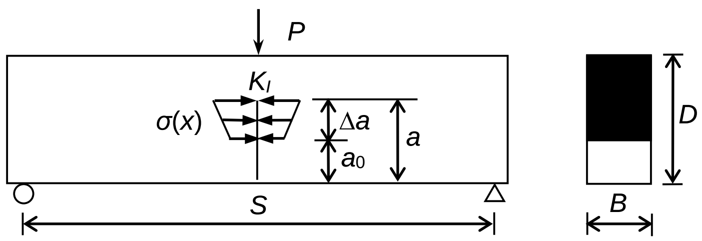

(a)

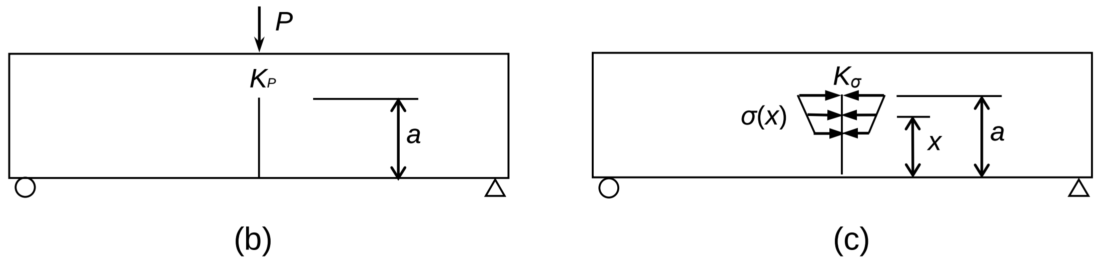

Fig. 1. Linear superposition method for calculating K_I

In the nil-SIF criterion[9], considering that the introduction of FPZ avoids the non-physical, singular stress fields at the fictitious crack tip, a crack can propagate once the driving force overcomes the resistance from the cohesive force, i.e. SIF at the fictitious crack tip K_I>0. However, there is a different point of view about the stress singularity at the fictitious crack tip in initial fracture toughness criterion[19]. According to the double-*K* theory[22, 23], for a beam under three-point bending with an initial crack length a_0, a crack does not initiate until the applied load P reaches the initial cracking load P_{ini}, i.e., the SIF at the tip of the crack reaches the initial fracture toughness K_{ini}. The crack propagation length Δa is assumed to be formed under the condition of the applied load $P>P_{ini}$. Then, the nonlinear behavior of concrete caused by crack propagation can be characterized by the fictitious cohesive stress acting on the FPZ according to the fictitious crack model. Upon this point, the beam under three-point bending with the initial crack length a_0 can be regarded as a beam with the initial crack length $a_0+\Delta a$ under the applied load P and fictitious cohesive force acting on the FPZ. Therefore, further crack propagation, which can also be regarded as a new crack initiation, will take place when the difference of SIFs caused by the applied load and fictitious cohesive force exceeds the initial fracture toughness K_{ini}, i.e., $K_I > K_{ini}$.

3. Analytical method for calculation of crack propagation

By the introduction of initial fracture toughness and nil-SIF criteria, the crack propagation of mode-I fracture in concrete can be calculated using an analytical method based on linear elastic fracture mechanics theory. The details of the numerical process are elaborated as following, in which a beam under three-point bending with initial crack length a_0 is taken as an example.

First, assuming a crack propagation length Δa, the new crack length a becomes $a_0+\Delta a$. Here, the SIF caused by the applied load can be determined by Eq. (2) [24].

$$K_P = \frac{3PS\sqrt{a}}{2D^2B}F_1(a/D) \tag{2}$$

Where, $F_1(a/D)$ can be defined by Eq.(3).

$$F_1(a/D) = \frac{1.99-(a/D)(1-a/D)[2.15-3.93(a/D)+2.7(a/D)^2]}{(1+2a/D)(1-a/D)^{3/2}} \tag{3}$$

The crack mouth opening displacement CMOD can be calculated by Eq. (4)[24].

$$CMOD = \frac{24P\lambda}{EB}\left[0.76-2.28\lambda+3.87\lambda^2-2.04\lambda^3+\frac{0.66}{(1-\lambda)^2}\right] \tag{4}$$

Where, E is the elastic modulus of concrete and λ is equal to $(a+H_0)/(D+H_0)$. H_0 is the thickness of the knife edge holding the clip gauges and equal to 2 mm in this study. Corresponding to the obtained $CMOD$, the crack opening displacement w at distance x from the crack mouth can be written as Eq. (5)[25].

$$w = CMOD\{(1-x/a)^2+[1.081-1.149(a/D)][x/a-(x/a)^2]\}^{1/2} \tag{5}$$

The relationship between the cohesive stress and crack opening displacement in the FPZ can be used to describe the softening behavior of concrete. Therefore, in this paper, a bilinear formulation[26] is employed to describe σ-w relationship which is mathematically presented as follows:

$$\sigma(x) = f_t - (f_t - \sigma_s)\frac{w}{w_s}, \ 0 \le w \le w_s \tag{6}$$

$$\sigma(x) = \sigma_s \frac{w_0 - w}{w_0 - w_s}, \ w_s \le w \le w_0 \tag{7}$$

$$\sigma(x) = 0, \ w \ge w_0 \tag{8}$$

where, f_t is the uniaxial tensile strength of concrete, w_0 is the displacement of the terminal point of σ-w curve beyond which no stress can be transferred, i.e. the stress-free crack width, w_s and σ_s is the displacement and stress, respectively, corresponding to the break point in the bilinear σ-w relationship, in which $\sigma_s = f_t/3$, $w_s = 0.8G_F/f_t$, $w_0 = 3.6G_f/f_t$. These parameters and the σ-w relationship can be derived given the fracture energy G_f and the uniaxial tensile strength f_t. Further, the SIF caused by cohesive forces σ(x) acting at the FPZ can be calculated by Eq. (9)[27].

$$K_\sigma = \int_{a_0}^{a} 2\sigma(x) F_2(x/a, a/D) / \sqrt{\pi a}\, dx \tag{9}$$

$F_2(x/a, a/D)$ can be defined by Eq. (10).

$$F_2(x/a, a/D) = \frac{3.52(1 - x/a)}{(1 - a/D)^{3/2}} - \frac{4.35 - 5.28(x/a)}{(1 - a/D)^{1/2}} + \left[\frac{1.3 - 0.3(x/a)^{3/2}}{\sqrt{1 - (x/a)^2}} + 0.83 - 1.76(x/a)\right] \times \left[1 - (1 - x/a)(a/D)\right] \tag{10}$$

Since K_P and K_σ can be obtained from Eqs. (2) and (9) for a beam under three-point bending, the appropriate load corresponding to the crack propagation length Δa can be found such that the propagation criterion $K_I > 0$ or $K_I > K_{ini}$ is satisfied. Therefore, the whole fracture process and *P-CMOD* curves can be obtained by repeating this exercise for each given crack propagation length, providing all material parameters, specifically K_{ini}, G_f, f_t and E are available from experiment.

4. Experimental program

To validate the two SIF-based criteria, five series of notched concrete beams, with different strength grades, i.e. C20, C40, C60, C80, C100 were tested under three-point bending and the corresponding *P-CMOD* curves were obtained. The beams in each series had the same dimensions, i.e. $S \times D \times B$=400 mm×100 mm× 40 mm, but the initial crack length/depth ratio a_0/D was equal to either 0.2, 0.3 or 0.4. For instance, the specimen number “TPB40-0.3” denotes a series of beams under three-point bending of C40 grade strength and a_0/D=0.3. The mix proportions of concrete with different strength grades are listed in Table 1. Crushed limestone with a maximum size of 20 mm was used as coarse aggregate for C20-C80 concrete. Crushed granite with a maximum size of 16 mm was used as coarse aggregate for C100 concrete. Medium-size river sand was used as fine aggregate. It should be noted that the C20 and C40 concretes were made with Grade R42.5 Portland cement (Chinese standard of Common Portland Cement, GB175-2007), and the C60, C80, and C100 concretes were made with Grade R52.5 Portland cement (Chinese standard of Common Portland Cement, GB175-2007). Meanwhile, in order to improve the workability of high strength concrete which has lower water-to-cement ratio, fly ash and water reducing admixture were added to the C60, C80, and C100 concrete.

Table1. Concrete mix proportions with different strength grades

Concrete	Cement grade	Cement	Sand	Aggregate	Water	Fly ash	Silica fume	Water reducing admixture
		(kg/m^3)						
C20	R42.5	336	692	1177	195	-	-	-
C40	R42.5	446	593	1102	214	-	-	-
C60	R52.5	390	631	1226	142	61	-	6.31
C80	R52.5	420	495	1155	144	120	60	13.4
C100	R52.5	420	495	1155	138	120	60	9

Engineering properties, including compressive strength, tensile strength and elastic modulus as well as fracture parameters including initial fracture toughness and fracture energy of the concrete prepared, are determined from relevant experiment / analysis and the results are listed in Tables 2 and 3. The initial fracture toughness is calculated using Eq. (2), in which the initial cracking load and initial crack length are employed accordingly. To measure the initial cracking load, four stain gauges were attached vertically in front of the precast notch on both sides of a beam, a distance of 10mm apart. The experimental setup for the three-point bending test is shown in Fig. 2. When a crack initiates and starts to propagate, measured strain will decrease suddenly and significantly from its maximum value due to a sudden release of fracture energy. Therefore, the initial cracking load can be obtained according to the variation of the strain around the tip of a pre-notch (See Fig. 3). According to [22, 23], the initial concrete fracture toughness is an inherent material property irrespective of effective crack length, so that the average of K_{ini} is given for beams under three-point bending with different a_0/D. The fracture parameters of concrete were measured according to the recommendation of RILEM TC 50[28].

Accordingly, the critical toughness K_{un} can be obtained by substituting the maximum load P_{max} and the critical cracking length a_c into Eq. (2). The critical crack length a_c for a beam under three-point bending can be calculated using Eq. (11) [23].

$$a_c = \frac{2}{\pi}(D+H_0)\arctan\left(\frac{B\cdot E\cdot CMOD_C}{32.6P_{\max}} - 0.1135\right)^{1/2} - H_0 \tag{11}$$

where, $CMOD_C$ is the critical crack mouth opening displacement, which can be measured in experiment.

Table 2. Engineering properties of concrete

Concrete	f_c (MPa)	f_t (MPa)	E (GPa)
C20	32.8	3.05	29.9
C40	48.9	3.74	33.2
C60	69.9	4.43	35.7
C80	84.1	5.01	38.1
C100	115.8	5.71	41.4

Table 3. Fracture parameters of beams under three-point bending

Nos.	a_C(mm)	K_{ini} (MPa·m$^{1/2}$)	K_{un}(MPa·m$^{1/2}$)	G_f (N/m)
TPB20-0.2	51	0.577	1.349	127.9
TPB20-0.3	60	0.461	1.127	117.1
TPB20-0.4	62	0.452	0.944	109.9
TPB40-0.2	43	0.634	1.242	130.6
TPB40-0.3	55	0.616	1.399	124.5
TPB40-0.4	63	0.559	1.043	111.8
TPB60-0.2	39	0.706	1.469	122.4
TPB60-0.3	50	0.632	1.444	114.9
TPB60-0.4	56	0.698	1.372	135.8
TPB80-0.2	45	0.854	1.729	141.0
TPB80-0.3	47	0.667	1.532	120.5
TPB80-0.4	65	0.735	1.398	110.8
TPB100-0.2	42	1.030	1.859	138.0
TPB100-0.3	48	0.917	1.806	115.4
TPB100-0.4	62	0.875	1.764	125.0

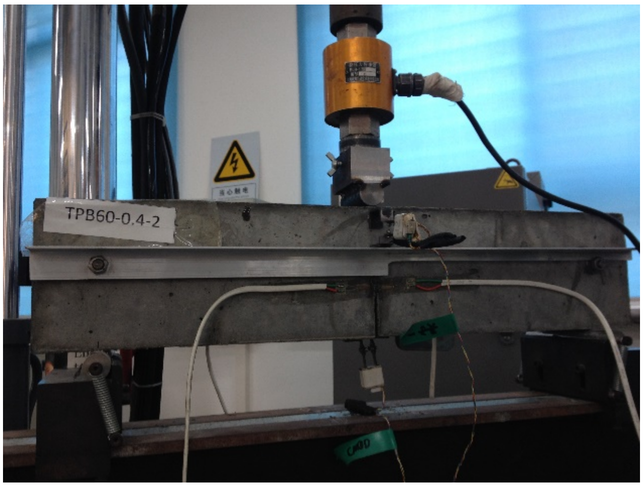

Fig. 2. Setup of a beam under the three-point bending

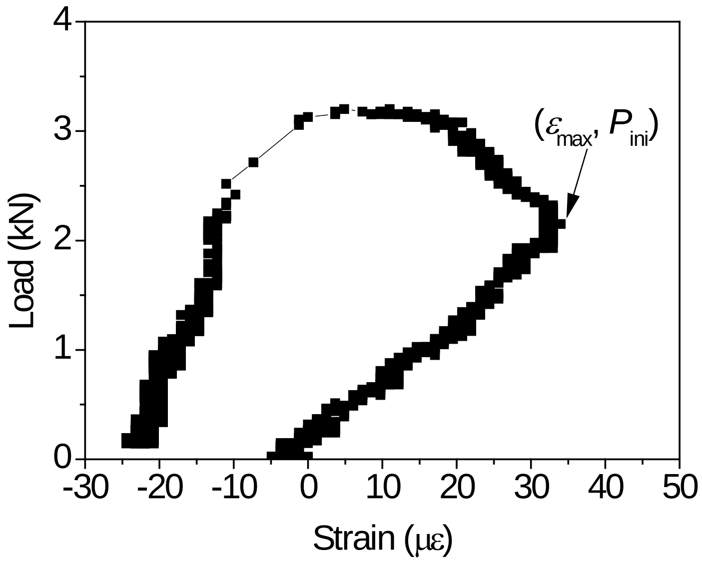

Fig. 3. Strain variation of concrete around crack tip

5. Results and discussion

The *P-CMOD* curves of the beams under three-point bending with different concrete strength grades were obtained from experiment, which are presented in Figs. 4 to 8. The corresponding *P–CMOD* curves obtained from numerical analysis using the nil SIF and the initial fracture toughness criteria are also presented in Figs. 4 to 8. It should be noted that for the beams under three-point bending with the same strength grade and a_0/D, the average values of material properties from experiment, including K_{ini}, G_f, E, f_t are used in the analytical solution. Taking series TPB40-0.3 as an example, there are five samples with C40 concrete and a_0/D=0.3, whose average values of K_{ini}, G_f, E and f_t are 0.616 MPa·m$^{1/2}$, 124.5 N/m, 33.2 GPa and 3.74 MPa, respectively (See Tables 1 and 2). Meanwhile, for the TPB40-0.3 series shown in the Fig 5 (b), the five curves with different gray levels denote the *P-CMOD* ones measured from experiment, and the red and blue highlighted curves denote the predicted *P-CMOD* ones based on the nil SIF and the initial fracture toughness criteria, respectively.

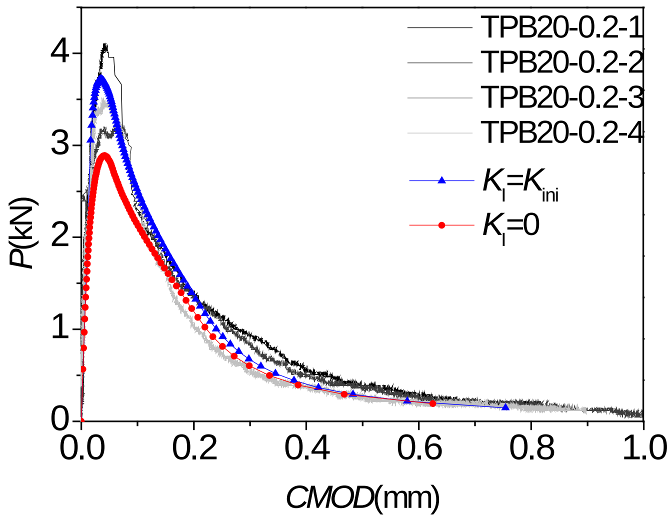

(a) Series of TPB20-0.2

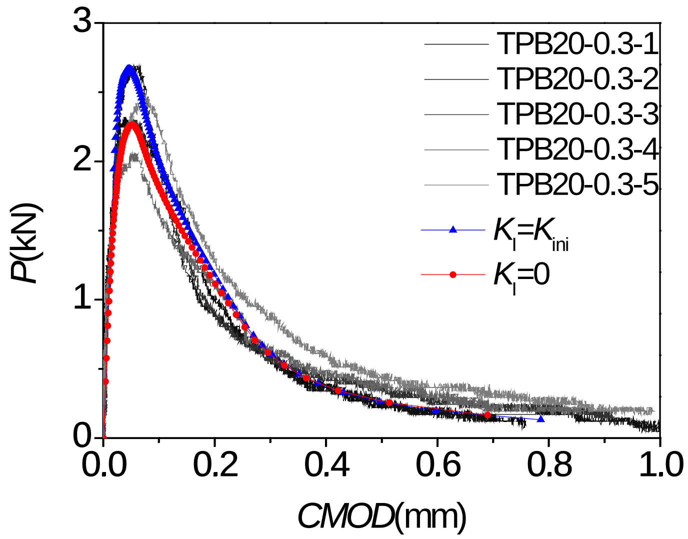

(b) Series of TPB20-0.3

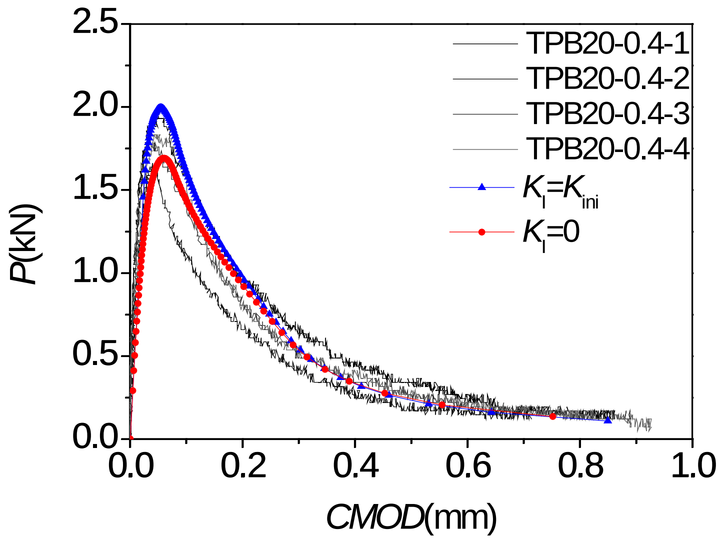

(c) Series of TPB20-0.4

Fig. 4. P-CMOD curves for C20 concrete

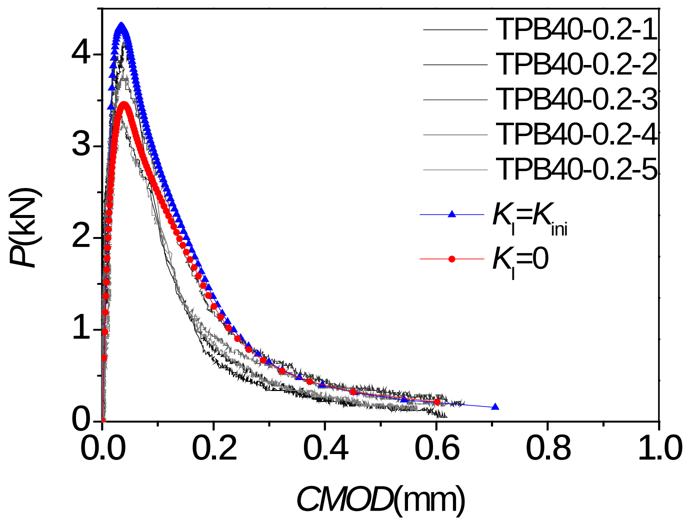

(a) Series of TPB40-0.2

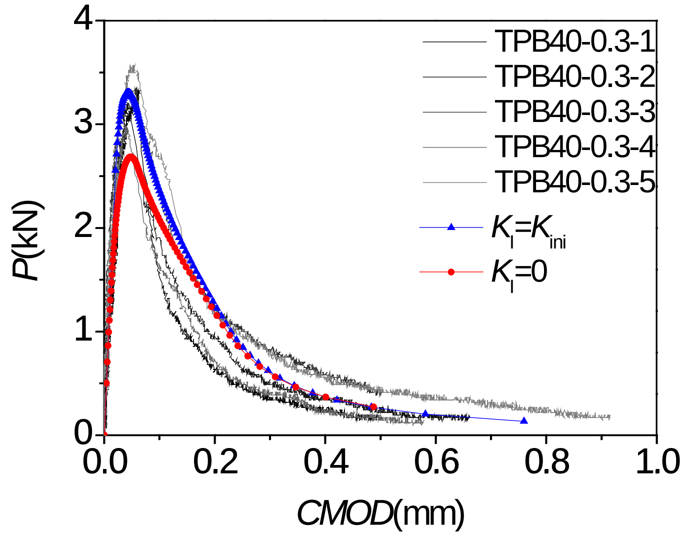

(b) Series of TPB40-0.3

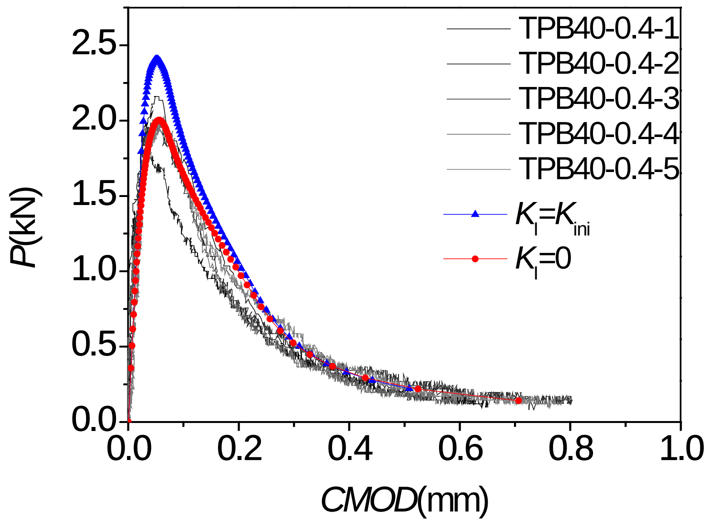

(c) Series of TPB40-0.4

Fig. 5. P-CMOD curves for C40 concrete

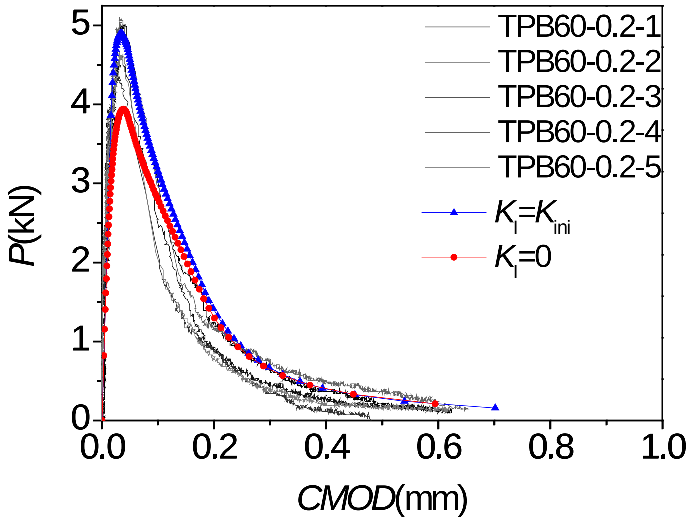

(a) Series of TPB60-0.2

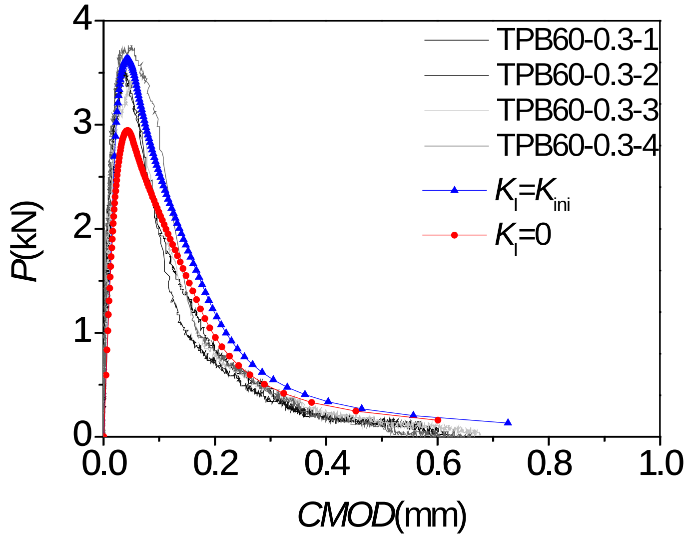

(b) Series of TPB60-0.3

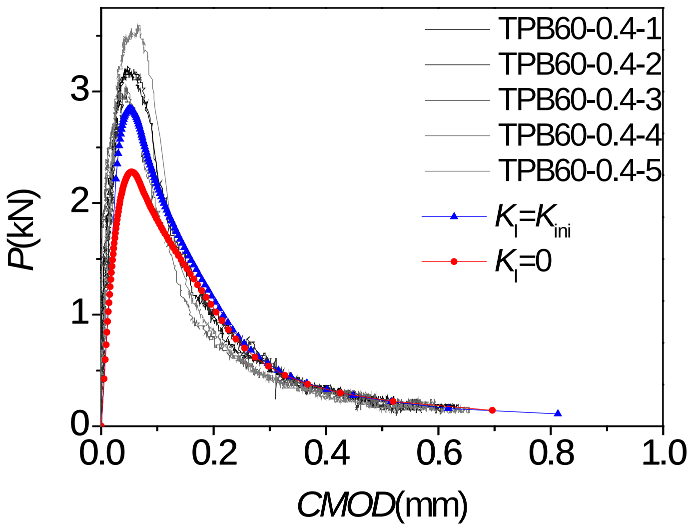

(c) Series of TPB60-0.4

Fig. 6. P-CMOD curves for C60 concrete

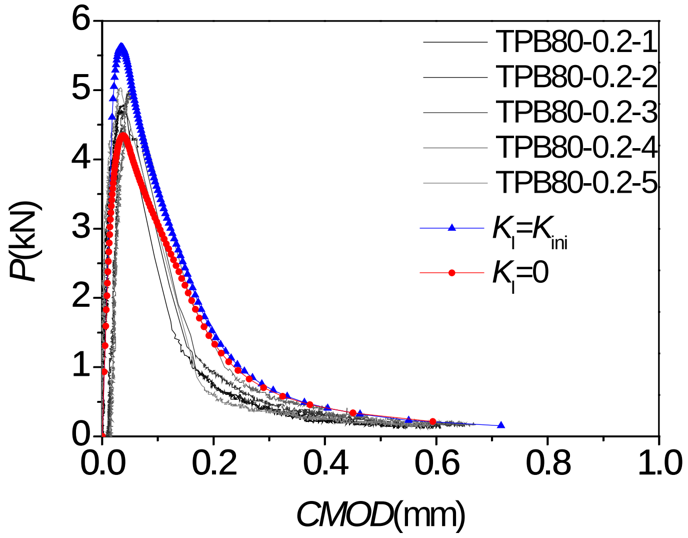

(a) Series of TPB60-0.2

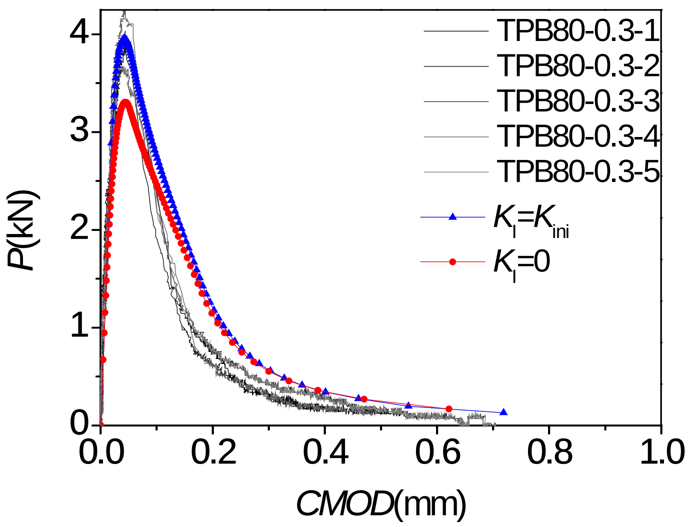

(b) Series of TPB40-0.3

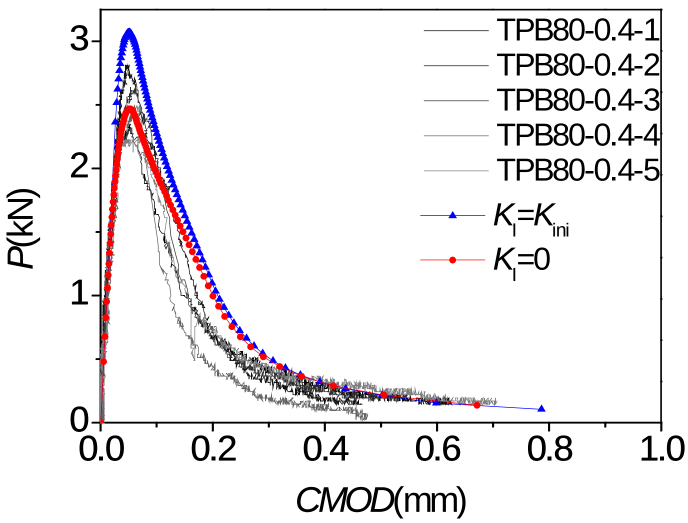

(c) Series of TPB80-0.4

Fig. 7. P-CMOD curves for C80 concrete

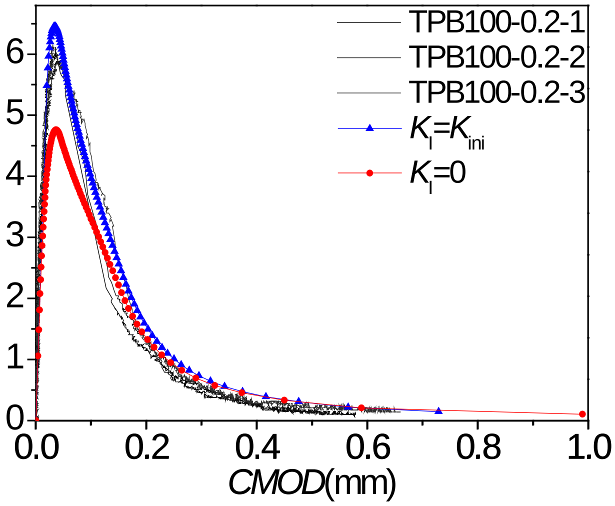

(a) Series of TPB100-0.2

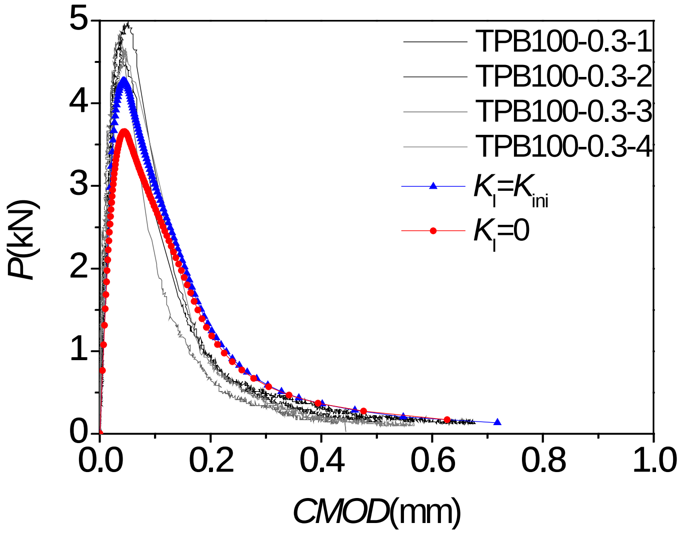

(b) Series of TPB100-0.3

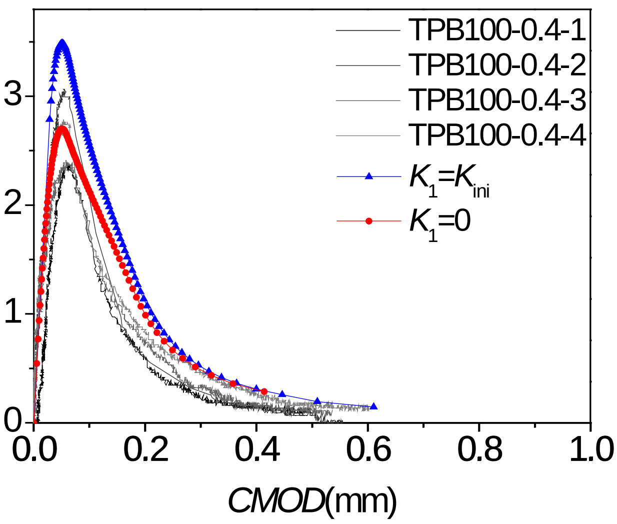

(c) Series of TPB100-0.4

Fig. 8. P-CMOD curves for C100 concrete

5.1 Influence of crack propagation criterion on P_{max}, a_C and $CMOD_C$

According to the *P-CMOD* curves shown in Figs. 4 to 8, it can be seen that the predicted *P-CMOD* curves from the two SIF-based criteria are almost within the envelope of experimental results. However, the calculated peak loads using the nil SIF criterion (i.e. K_I=0) are significantly less than the one using the initial fracture toughness criterion (i.e. K_I=K_{ini}). This can be explained by analyzing the fracture mechanism implied by the two SIF-based criteria. In fact, there is an essential difference on the assessment of propagation resistance at the tip of fictitious crack in these two criteria to predict the fracture process of concrete. In the nil SIF criterion, the crack propagation resistance is caused by the cohesive force action on the FPZ. In contrast, in the initial fracture toughness criterion (i.e. K_I=K_{ini}), the crack propagation resistance is caused by the cohesive force action on the FPZ as well as the initial fracture toughness K_{ini}. When the peak load is reached, the SIF at the tip of a fictitious crack is equal to the critical fracture toughness K_{un}, which can be regarded as a material property. If denoting the calculated critical crack length using the nil SIF and the initial fracture toughness criteria as a_{c1} and a_{c2}, respectively, the following relationship can be obtained.

$$K_\sigma(a_{c1})=K_{ini}+K_\sigma(a_{c2})=\mathrm{K}_{un} \quad (12)$$

Where, $K_\sigma(a_{c1})$ and $K_\sigma(a_{c2})$ are the SIFs caused by the cohesive force corresponding to the critical crack length a_{c1} and a_{c2}. It can be seen from Eq. (12) that $K_\sigma(a_{c1})>K_\sigma(a_{c2})$, given the same set of material parameters for a certain type of concrete, the relationship of $a_{c1}> a_{c2}$ can be obtained according to Eq. (9), i.e. the critical crack length based on the nil SIF criterion is greater than the one based on the initial fracture toughness criterion. Further, according to Eq. (2), it can be concluded that the calculated peak load based on the nil SIF criterion is less than the one based on the initial fracture toughness criterion.

A comparison is made between the predicted peak loads based on the two SIF-based criteria and the experimental ones as shown in Fig. 9. In this figure, the average value of peak loads from experiment is taken for the beams under three-point bending with the same strength grades and a_0/D. Three beams with the same concrete grade and a_0/D were tested in experiment. The horizontal axis $P_{\max,\mathrm{pre}}$ represents the calculated peak load and the vertical axis $P_{\max,\mathrm{exp}}$ represents the measured peak load from experiment. It can be seen that the predicted peak load using the $K_\mathrm{I}=K_\mathrm{ini}$ criterion is much closer to the experimental results than that using the $K_\mathrm{I}=0$ criterion. Compared with the experimental results, most of the predicted peak loads using the $K_\mathrm{I}=0$ criterion are underestimated. Meanwhile, a comparison of critical crack length is made between the theoretical results from Eq. (11) and predictions as shown in Fig. 10. In Eq. 11, the average values of $CMOD_\mathrm{C}$ from experiment are used to calculate a_C for the beams in three-point bending with the same strength grade and a_0/D. The horizontal axis $a_{\mathrm{C,pre}}$ represents the calculated critical crack length from numerical analysis and the vertical axis $a_{\mathrm{C,cal}}$ represents the theoretical critical crack length from Eq. (11). It can be seen that the predicted critical crack length using the $K_\mathrm{I}=K_\mathrm{ini}$ criterion is much closer to the theoretical results than that using the $K_\mathrm{I}=0$ criterion. Compared with the theoretical results, most of the predicted critical crack length using the $K_\mathrm{I}=0$ criterion is overestimated. Accordingly, the critical crack mouth opening displacement $CMOD_\mathrm{C}$ can be measured using the clip setting on the bottom of a beam under three-point bending (see Fig. 2). A comparison of $CMOD_\mathrm{C}$ is made between the measured results from the experiment and calculated results as shown in Fig. 11. The horizontal axis $CMOD_{C,pre}$ represents the calculated critical crack mouth opening displacement and the vertical axis $CMOD_{C,exp}$ represents the measured one from experiment. It can be seen that the predicted $CMOD_C$ using the K_I=K_{ini} criterion is much closer to the measured results than that using the K_I=0 criterion. Compared with experimental results, the predicted $CMOD_C$ using the K_I=0 criterion is a slight overestimation.

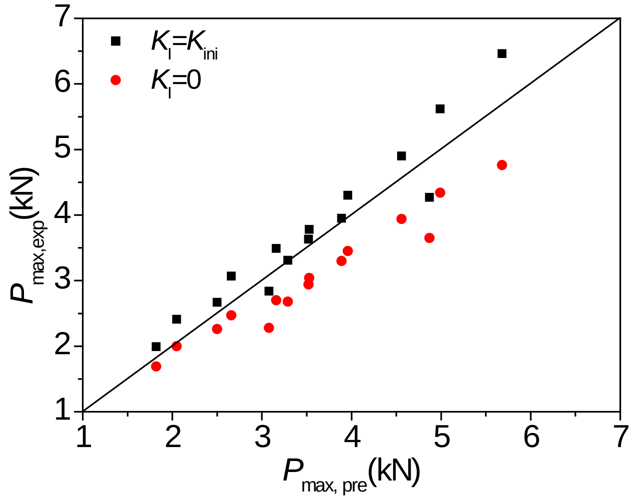

Fig. 9. P_{max} obtained from experiment and prediction

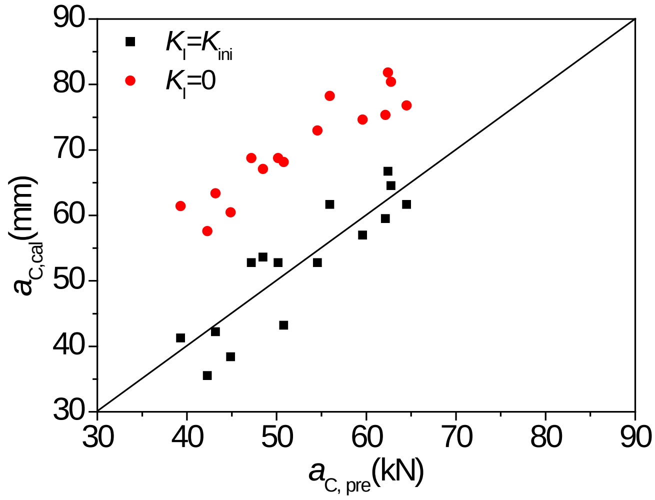

Fig. 10. a_C obtained from theoretical analysis and prediction

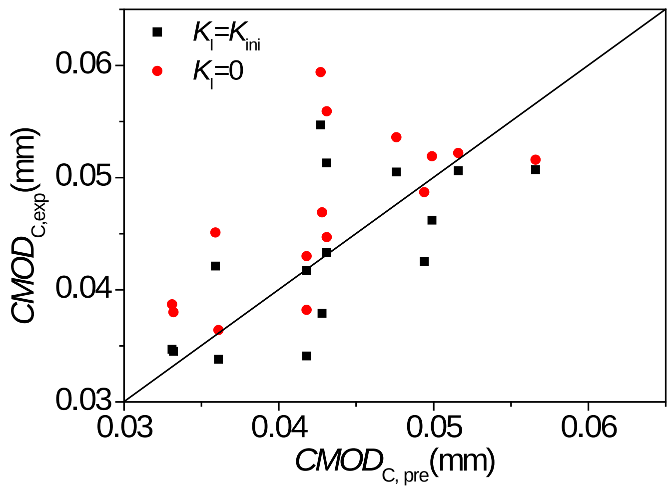

Fig. 11. *CMOD*$_C$ obtained from experiment and prediction

5.2 Influence of concrete strength on predicted results

For a perfect plastic material, the resistance to structural deformation is caused by its cohesion. The concept of fracture toughness based on the LEFM does not work for plastic materials which exhibit nonlinear properties. Therefore, the initial fracture toughness K_{ini} can be regarded as zero for plastic materials. Due to this, the nil SIF criterion and the initial fracture toughness criterion have the same expression, i.e. K_I>0. In this study, the SIF-based criteria is not intended to be used for analyzing crack propagation in a plastic material, but rather for describing the formal transformation of the two criteria when they are employed in the analysis of materials with different brittleness. Accordingly, for a perfectly brittle material, there is no crack propagation process, i.e. the crack will propagate throughout the section of specimen once it initiates. In this case, the FPZ cannot be formed, and cohesive forces do not exist within the material. Therefore, the unique resistance of crack propagation is provided by the initial fracture toughness K_{ini}, which is equal to the critical toughness K_{un}. Upon this point, the initial fracture toughness criterion can be expressed as K_I>K_{ini}=K_{un}, which has a good agreement with the fracture criterion used in LEFM. However, the nil SIF criterion K_I>0 is not applicable under this condition, as it will lead to an unreasonable result, i.e., a crack can propagate continuously under even a tiny accidental load.

In a quasi-brittle material such as concrete, the nonlinear behavior in load vs. deformation curve of a beam under three-point bending is caused by the crack propagation together with the cohesive stress along FPZ. In contrast to perfectly brittle materials, the length of this process zone is usually not negligible compared to the size of a typical structure. With the increase of concrete strength, the brittleness of concrete increases which results in shortening of the whole FPZ length and the enhancement of initial fracture toughness in concrete. Fig. 12 illustrates the variation of the FPZ length during the fracture process. Through a comparison of FPZ variation among concretes with various strength grades, it can be seen that the whole FPZ length is much shorter for the specimens with a higher strength grade when a certain criterion is adopted, which reflects the effect of brittleness on a material’s fracture properties. Meanwhile, through a comparison of FPZ evolution based on the two criteria, it can be seen that the FPZ length is much longer after the whole PFZ is formed with respect to the nil SIF criterion than that with respect to the initial fracture toughness criterion. It can be explained that, for the nil SIF criterion, a much longer PFZ is necessary for the purpose of balance between driving force caused by external load and resistance caused by cohesive force acting on the PFZ. With the increase of concrete strength, the difference in the whole FPZ length based on the two criteria becomes increasingly larger (see Figs. 12 (a) to (c)), as the decrease of FPZ length is more significant for higher strength concrete when initial fracture toughness criterion is adopted.

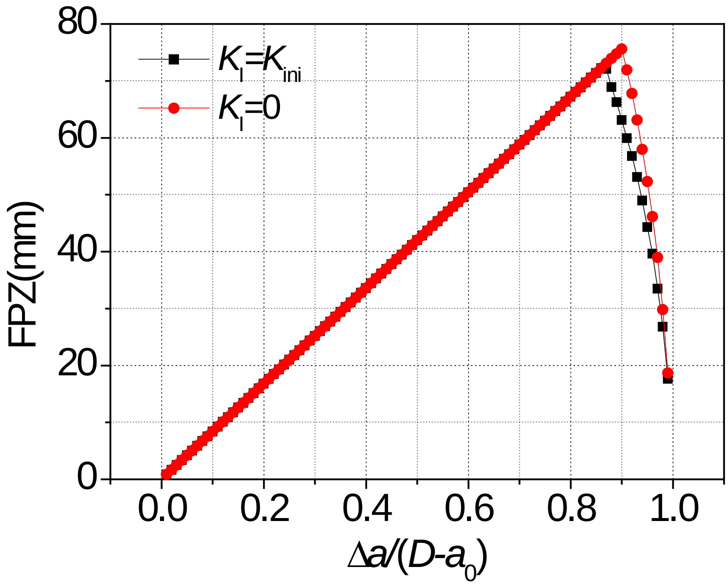

(a) TPB20-0.3

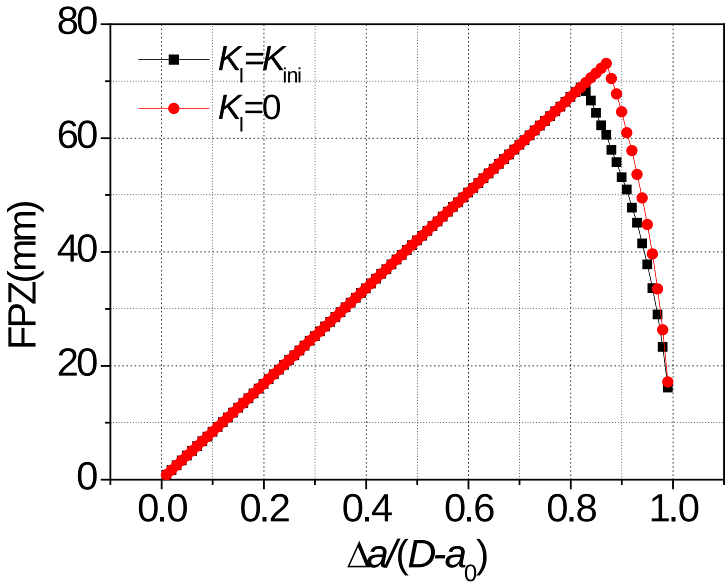

(b) TPB60-0.3

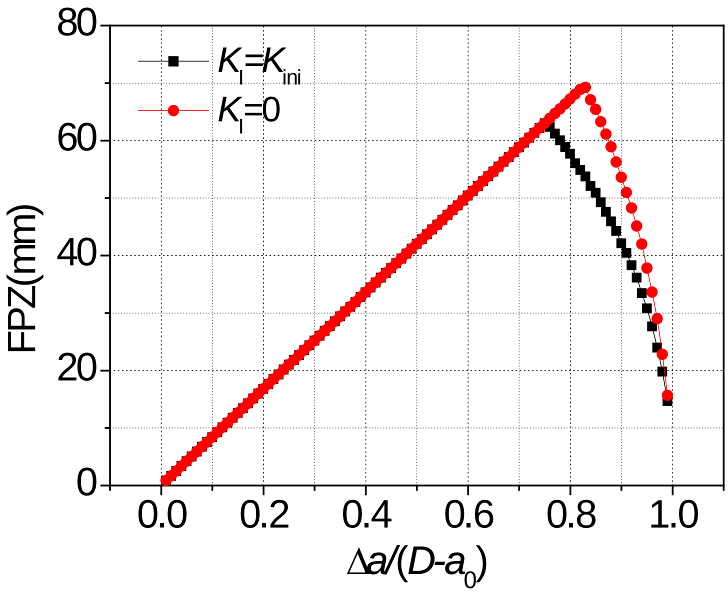

(c) TPB100-0.3

Fig. 12. Variation of FPZ of concrete with different strength

Fig. 13 illustrates the K_R-resistance curves calculated by the two criteria. The method for constructing the K_R-resistance curves refers to [19], in which the equation of K_R=K_P is adopted in both criteria. It can be seen that, at the beginning of crack propagation, the difference of resistance in the two criteria is equal to the initial fracture toughness K_{ini}. With the increase of crack propagation length, the difference of K_R curves becomes increasingly smaller until the two curves meet at a point, which is denoted by a hollow circle in Fig. 13. For the C20, C60 and C100 concretes, the values of $\Delta a/(D-a_0)$ at the intersection of two curves are 0.5, 0.6 and 0.65, respectively. It indicates that the initial fracture toughness has a significant effect on the crack propagation resistance at the early stage of cracking, which leads to a higher resistance when using the initial fracture toughness criterion in fracture analysis. However, with the increase of crack propagation length, instead of the initial fracture toughness, the cohesive force becomes more significant, which results in the higher resistance when the nil SIF criterion is adopted in fracture analysis. The corresponding peak loads in K_R curves are denoted by solid red and green circles in Figs. 13 (a) to (c), with respect to the nil SIF and initial fracture toughness criteria, respectively. It indicates that, for low strength concrete, e.g., the C20 concrete in Fig. 13 (a), the difference in K_R curves is not significant, as the initial fracture toughness is small. The intersection of the two curves appears at the post-peak load stage for the initial fracture toughness criterion, but at the pre-peak load stage for the nil SIF criterion. For the normal and high strength concretes, e.g., the C60 and C100 concretes in Figs. 13 (b) and (c), the difference in the K_R curves is more significant. The intersection of the two curves appears at the post-peak load stage for both criteria. Compared with the normal strength concrete, the intersection of the two curves in high strength concrete is far away from the peak load points. Therefore, for a higher strength concrete, using the initial fracture toughness criterion, the calculated resistance is larger causing the crack propagation process to take much longer than using the nil SIF criterion.

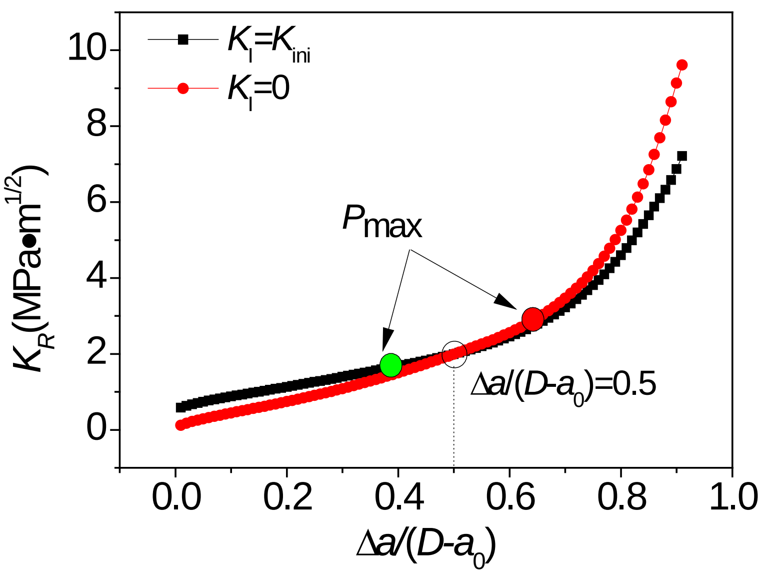

(a) TPB20-0.3

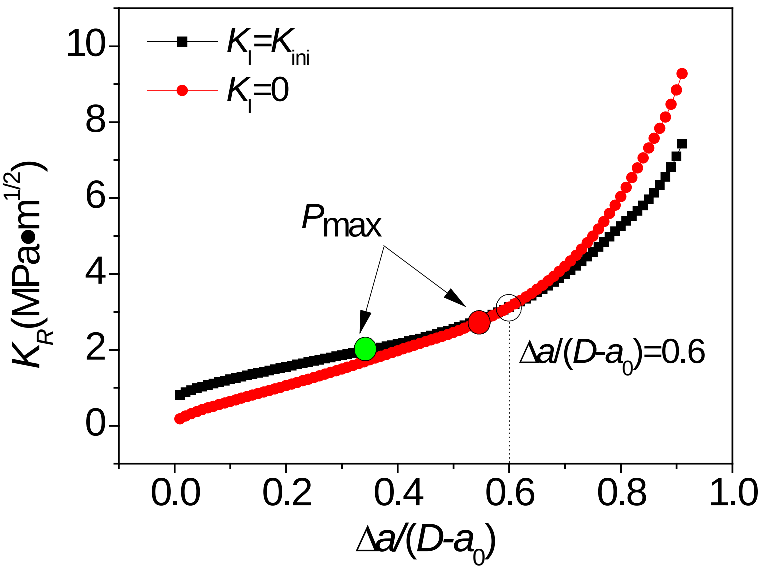

(b) TPB60-0.3

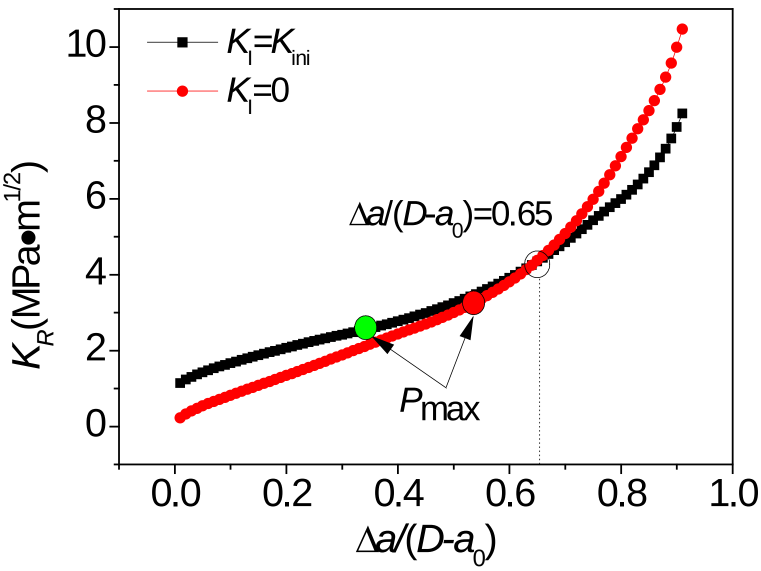

(c) TPB100-0.3

Fig. 13. K_R curves of concrete with different strength

Meanwhile, with the increase of the concrete strength, the initial fracture toughness increases, accordingly. Taking the C20 and C100 concrete as examples, the initial fracture toughness is approximately 0.5 MPa·m$^{1/2}$ and 0.94 MPa·m$^{1/2}$, respectively, i.e. the value is almost doubled from C20 to C100 concrete. Due to the short critical crack propagation length, the initial fracture toughness has a significant effect on crack propagation resistance length when the peak load is reached. Also, the initial fracture toughness plays an increasingly more significant role in crack propagation with the increase of concrete strength. Since the effect of the initial fracture toughness on crack propagation is not considered in the nil-SIF criterion, the difference in P_{max} between the predicted and experimental values could increase with the increase of concrete strength. As an output of this comparison, Fig. 14 illustrates P_{max} errors between predicted and experimental results using the two criteria for concrete with different strength grades. As expected, the errors of P_{max} from the nil-SIF criterion are always larger than the ones from the initial fracture toughness criterion, and the error increases with the increase of concrete strength. It should be noted that the tendency of error variation is not obvious for the results of the C80 concrete, which can be explained by the wide discreteness, elaborated as following. According to experimental results, the P_{max} of the beam under three-point bending with a_0/D=0.4 is 2.65 kN in the C80 concrete, and 3.08 kN in the C60 concrete is. Therefore, in general, the prediction using the initial fracture toughness criterion shows a better agreement with the experimental results than using the nil-SIF criterion. Also comparing with the nil-SIF criterion, the advantage of the initial fracture toughness criterion is more significant with the increase of concrete strength grade.

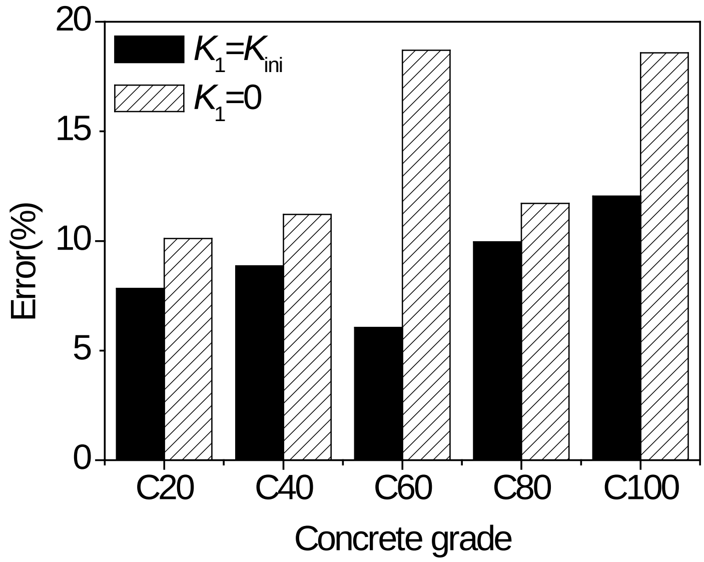

Fig.14. P_{max} error for concrete with different strength grades

6. Conclusions

Two SIF-based criteria, nil-SIF and the initial fracture toughness, were adopted to determine crack propagation and analytical solutions were presented based on the two criteria to calculate the whole fracture process of concrete. Meanwhile, a series of beams under three-point bending with different a_0/D and concrete strength grades were tested to obtain *P-CMOD* curve. Comparing with the experimental results, the predicted results obtained by employing the two SIF-based criteria showed different degrees of agreement. Further, the effects of different crack propagation criteria on predicted results, including P_{max}, a_C and $CMOD_C$, were investigated. Finally, from the point of view of exploring the fracture mechanism, the K_R-resistance curves and FPZ were calculated and the effects of concrete strength on the predicted results using the two SIF-based criteria were investigated. The following conclusions can be drawn:

(a) The two SIF-based criteria can be used for calculating crack propagation of concrete through combination with the fictitious fracture model. Comparing with experimental results, the predicted P_{max}, a_C and $CMOD_C$ based on the initial fracture toughness criterion show a better agreement than the ones from the nil-SIF criterion. With respect to the nil-SIF criterion, the predicted P_{max} values are underestimated, but a_C and $CMOD_C$ are overestimated when compared with experimental results.

(b) With the increase of concrete strength, the initial fracture toughness plays an increasingly more significant role in the evaluation of crack propagation resistance, especially for the pre-peak load stage. The K_R-curves obtained from the two criteria are different, with the one obtained from the initial fracture toughness criterion being higher than that from the nil-SIF criterion at the early stage of crack propagation, however the opposite case is observed at the late stage of crack propagation.

(c) Although the errors of predicted peak load show a smaller difference for low strength concrete when adopting the two SIF-based criteria, the differences are more significant with the increase of concrete strength. Therefore, for high strength concrete, the initial fracture toughness criterion is more appropriate than the nil-SIF criterion in determining the crack propagation process.

Acknowledgement

The financial support of the, the National Natural Science Foundation of China under the grant of NSFC 51478084, 51421064 and 51478083, and the fundamental research funds for the Central Universities under the grant of DUT14LK06 is gratefully acknowledged.

References

[1] Hillerborg A, Modéer M, Petersson PE. Analysis of crack formation and crack growth in concrete by means of fracture mechanics and finite elements. Cem Concr Res. 1976;6:773-81.

[2] Wells GN, Sluys LJ. A new method for modelling cohesive cracks using finite elements. Int J Numer Meth Eng. 2001;50:2667-82.

[3] Shi Z, Ohtsu M, Suzuki M, Hibino Y. Numerical Analysis of Multiple Cracks in Concrete Using the Discrete Approach. Journal of Structural Engineering. 2001;127:1085-91.

[4] Shi Z. Numerical Analysis of Mixed-Mode Fracture in Concrete Using Extended Fictitious Crack Model. Journal of Structural Engineering. 2004;130:1738-47.

[5] Xie M, Gerstle WH. Energy-Based Cohesive Crack-Propagation Modeling. Journal of Engineering Mechanics-Asce. 1995;121:1349-58.

[6] Yang ZJ, Chen JF. Finite element modelling of multiple cohesive discrete crack propagation in reinforced concrete beams. Eng Fract Mech. 2005;72:2280-97.

[7] Yang ZJ, Chen JF. Fully automatic modelling of cohesive discrete crack propagation in concrete beams using local arc-length methods. Int J Solids Struct. 2004;41:801-26.

[8] Yang ZJ, Proverbs D. A comparative study of numerical solutions to non-linear discrete crack modelling of concrete beams involving sharp snap-back. Eng Fract Mech. 2004;71:81-105.

[9] Moës N, Belytschko T. Extended finite element method for cohesive crack growth. Eng Fract Mech. 2002;69:813-33.

[10] Ooi ET, Yang ZJ. Modelling crack propagation in reinforced concrete using a hybrid finite element-scaled boundary finite element method. Eng Fract Mech. 2011;78:252-73.

[11] Ooi ET, Yang ZJ. A hybrid finite element-scaled boundary finite element method for crack propagation modelling. Comput Method Appl M. 2010;199:1178-92.

[12] Yang ZJ, Deeks AJ. Fully-automatic modelling of cohesive crack growth using a finite element-scaled boundary finite element coupled method. Eng Fract Mech. 2007;74:2547-73.

[13] Ooi ET, Yang ZJ. Modelling multiple cohesive crack propagation using a finite element-scaled boundary finite element coupled method. Eng Anal Boundary Elem. 2009;33:915-29.

[14] Foote RML, Mai Y-W, Cotterell B. Crack growth resistance curves in strain-softening materials. J Mech Phys Solids. 1986;34:593-607.

[15] Zhang J, Li VC. Simulation of crack propagation in fiber-reinforced concrete by fracture mechanics. Cem Concr Res. 2004;34:333-9.

[16] Li S, Thouless MD, Waas AM, Schroeder JA, D. ZP. Use of a cohesive-zone model to analyze the fracture of a fiber-reinforced polymer-matrix composite. Kidlington, ROYAUME-UNI: Elsevier; 2005.

[17] Mai Y-W. Cohesive zone and crack–resistance (R)-curve of cementitious materials and their fibre-reinforced composites. Eng Fract Mech. 2002;69:219-34.

[18] Wu Z, Rong H, Zheng J, Dong W. Numerical Method for Mixed-Mode I–II Crack Propagation in Concrete. J Eng Mech. 2013;139:1530-8.

[19] Dong W, Wu Z, Zhou X. Calculating crack extension resistance of concrete based on a new crack propagation criterion. Constr Build Mater. 2013;38:879-89.

[20] Dong W, Zhou X, Wu Z. On fracture process zone and crack extension resistance of concrete based on initial fracture toughness. Constr Build Mater. 2013;49:352-63.

[21] Qing LB, Tian WL, Wang J. Predicting unstable toughness of concrete based on initial toughness criterion. Journal of Zhejiang University-Science A. 2014;15:138-48.

[22] Xu SL, Reinhardt HW. Determination of double-K criterion for crack propagation in quasi-brittle fracture, Part I: Experimental investigation of crack propagation. Int J Fract. 1999;98:111-49.

[23] Xu S, Reinhardt HW. Determination of double-K criterion for crack propagation in quasi-brittle fracture, Part II: Analytical evaluating and practical measuring methods for three-point bending notched beams. Int J Fracture. 1999;98:151-77.

[24] Tada H, Paris PC, Irwin GR. The Stress Analysis of Cracks Handbook. New York, USA: ASME; 2000.

[25] Jenq Y, Shah S. Two Parameter Fracture Model for Concrete. J Eng Mech. 1985;111:1227-41.

[26] Petersson PE. Crack growth and development of fracture zones in plain concrete and similar materials. SWEDEN: Lund Institute of Technology; 1981.

[27] Jenq YS, Shah SP. A Fracture toughness criterion for concrete. Eng Fract Mech. 1985;21:1055-69.

[28] RILEM TCS 50. Rilem TC 50-FMC recommendation: Determination of the fracture energy of mortar and concrete by means of three-point bend tests on notched beams. Mater Struct. 1985;18:287-90.